Microwave Review
December 2024, Vol. 30, No. 2, pp. 15-22
DOI: 10.18485/mtts_mr.2024.30.2.2

Meta-Material Inspired Circularly Polarized Semi-Circled Fractal Boundary Antenna for Broadband and Multiband Applications

V. Venkateshwar Reddy[1], Suman Nelaturi[2], Rama Sanjeev B R[3], Sulakshana N[4]

Abstract – **For wireless applications, a meta-material loaded circularly polarized (CP) semi-circled fractal antenna is suggested. In order to construct the semi-circled CP antennas, semi-circled fractal curves are initially placed along the sides of a square patch. Then, to increase the CP bandwidth, meta-material reactive impedance surfaces (RIS) are loaded onto semi-circled circularly polarized antennas. The RIS patch elements are optimized to 5×5 for improving the CP bandwidth. The 10-dB impedance and 3-dB axial ratio (AR) bandwidths obtained by the proposed iteration 1 semi-circled fractal RIS antenna are 42.4% and 4.77%, respectively. A meta-material inspired multiband antenna working at WLAN - 2.45 GHz frequency and Wi-MAX 3.4 GHz frequency is also proposed by embedding 450 rotated mushroom unit cell at the centre of the suggested RIS patch for broadband operation. The newly designed multiband antenna achieves a 20.4% impedance bandwidth at WLAN application and an 18.18% bandwidth at Wi-MAX application, surpassing existing designs found in open literature. This RIS broadband antenna also demonstrates exceptional circular polarization (CP), wide return loss and axial ratio bandwidth.**

Keywords – **Meta-material, Semi-circled fractal, Reactive impedance surface, Circular Polarization.**

I. INTRODUCTION

Low-profile antennas are necessary for high-performance satellite, aircraft, missile, and spacecraft applications where ease of installation, size, performance, weight, aerodynamic profile, and cost are constraints. Similar standards are already used by many other governmental and commercial applications, including advanced wireless communications and mobile radio. These requirements can be met by using microstrip antennas. Metamaterials are man-made materials with unusual and favourable features. The engineering and physical scientific groups now share a tremendous excitement for exploration that they have helped to nurture. Several guiding and radiating structures have been used [1]. A class of antennas termed metamaterial-based antennas is inspired by metamaterials to improve the performance or perform novel functionality. They are recommended as an alternative because of their compact physical size, cheap cost, wide bandwidth, and high efficiency. Meta-surface, a subfield of metamaterials, has found extensive use in microwave circuits and antennas. There are various forms of meta-surfaces, including the RIS made up of periodic metallic patches, the artificial magnetic conductor that resembles a mushroom in terms of high impedance, and the uniplanar compact photonic band gap surface [2]. Ryan et al have proposed low-cost-meta-material-based transparent CP antennas [3]. Liu et al have presented a low-profile single, dual-layer wideband meta-surface antenna [4]. Cao et al have presented a method using I-shaped resonant meta-material for designing electrically large property microstrip-line slot antenna [5]. Chatterjee et al have nominated a RIS-based H-shaped broadband CP antenna [6]. Li et al have demonstrated a bidirectional, wideband, compact antenna by employing index gradient patches [7]. It consists of launcher element printed dipole and index-fixed, index-modulated patch as meta-surface for improving gain and bandwidth. Chen et al have examined a high-gain, wideband CP mushroom meta-material antenna [8]. It consists of 4×4 mushroom cells as meta-surface and an L-shaped slot coupling fed-layer. A mushroom meta-surface is employed to generate wideband CP radiation. Pan et al have designed low-profile UWB CP slot antennas [9]. Cao et al have suggested an electrically large property (ELP) microstrip antenna with SRR structures as meta-surface for improving the bandwidth [10]. Zhang et al have proposed meta-surface-based compact antennas [11]. Here the CPW monopole antenna is employed as a feeding structure for the compact meta-surface. Wan et al have implemented a patch-driven meta-surface antenna with low-profile broadband characteristics [12]. The presented antenna consists of the artificial magnetic conductor as the meta-surface with an aperture-coupled patch. Wang et al have studied an SRR-inspired periodically structured meta-surface, miniaturized CP antenna for RFID application [13]. Wu et al have presented a dual-band WLAN antenna by employing a meta-material structure [14]. Suman et al have investigated multiband antennas based on meta-material. However, the antennas they introduced demonstrated narrow return loss bandwidth across multiple bands [15]-[17]. Likewise, many of the existing designs in open literature exhibits less return loss bandwidth. In the proposed antenna, when a 45^0 rotated fractal patch embedded at the centre of the semi-circled fractal patch, impedance matching is done over a larger frequency range and so exhibits high bandwidth at both the bands. Fractal geometries are employed to microstrip patch antennas for

Article history: Received February 14, 2024; Accepted June 10, 2024

[1]V.Venkateshwar Reddy is with the Department of ECE, Kakatiya Institute of Technology and Science, Warangal, India. E-mail: vvr.ece@kitsw.ac.in.

[2]Suman Nelaturi is with the Department ECE, VFSTR, Guntur, India. E-mail: nelaturi.suman@gmail.com.

[3]Rama Sanjeev B R is with the Department of ECE, BVRIT, Narsapur, India. E-mail: sanjeev.reddy@bvrit.ac.in.

[4]Sulakshana. N is with the Department of ECE, Vardhaman College of Engineering, Hyderabad, India. E-mail: sulakshana@vardhaman.com

designing compact antennas. While previous studies mainly applied RIS to linearly polarized conventional patch structures, this paper introduces RIS based CP fractal antennas. By incorporating fractal mushroom unit cell, multiband operation is achieved. Initially, single-band linearly polarized fractal antennas of iteration order 1 (IO1) and iteration order 2 (IO2) were developed, followed by CP antennas. To further widen the CP bandwidth, RIS is integrated, utilizing both square and fractal elements, resulting in a significant increase in bandwidth. Moreover, in pursuit of multiband operation with broad return loss bandwidth, RIS with scaled down and 45^0 rotated fractal mushroom unit cell is inserted at the centre of the semi-circled fractal boundary patch for the first time. Extensive simulations are performed on IO1 and IO2 antennas, demonstrating that the proposed multiband design showcases wide return loss bandwidth across both the operating bands. As compared to the existing literature the proposed antennas exhibit high impedance bandwidth at both the WLAN and Wi-MAX application bands.

II. PROPOSED ANTENNA

Figure 1 illustrates the development of the Semi-circled fractal for various iteration orders (IO), where R is the indentation radius. All of the patches' end-to-end lengths are taken into account to be 36 mm, allowing antennas to resonate in the 2GHz–3GHz frequency. Figure 2 depicts the proposed broadband antenna geometry. Figure 3 shows the presented multiband antenna geometry. In the beginning, an ISM band square patch antenna was created. Then, to implement linear and circularly polarised CP antennas, the square patch's edges are replaced out for semi-circled fractal curves. Later, these semi-circled antennas are loaded with RIS metamaterial for enhancing the CP bandwidth.

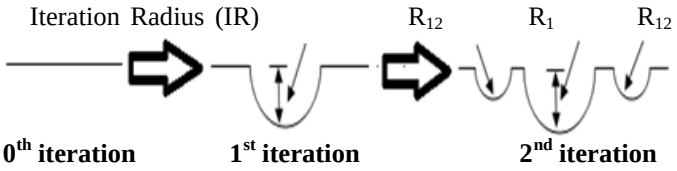

Fig. 1. Semi-circled fractal curve generation

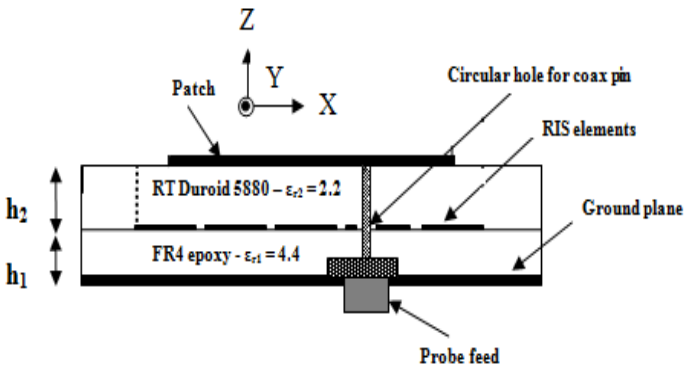

(a)

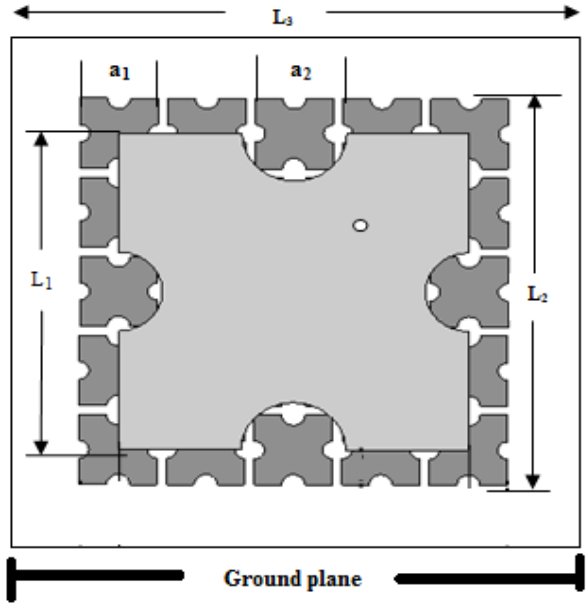

(b)

Fig. 2. The nominated broadband antenna geometry: (a) Side view, (b) Top view

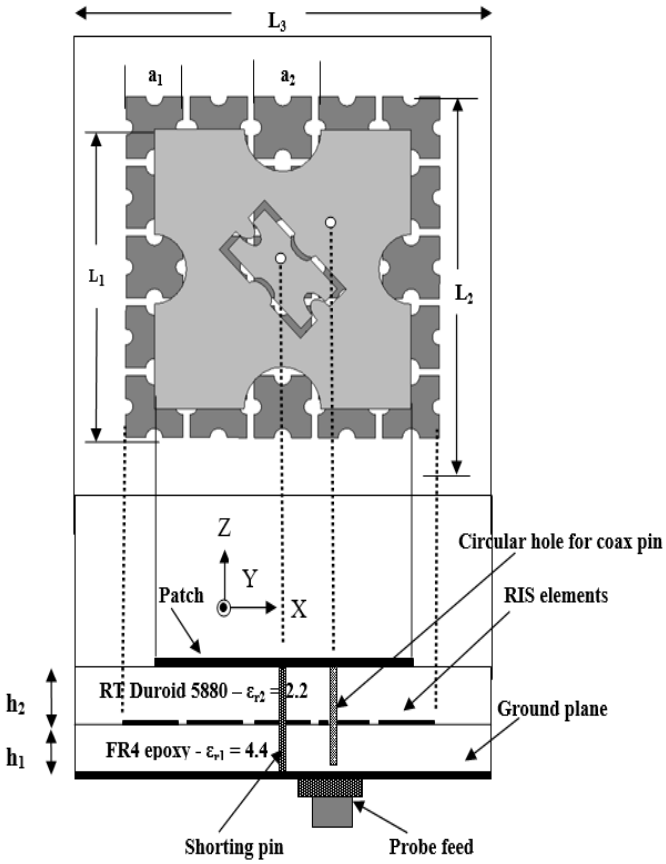

Fig. 3. The nominated multiband antenna geometry

III. SIMULATION RESULTS

The nominated microstrip antenna comprises of semi-circled IO1/IO2 patch implemented over dual layer substrates with bottom layer height h_1 as 1.6mm and top layer height h_2

as 3.2 mm. The RIS layer is made up of a series of metallic patches. The proposed antenna fed with probe feed mechanism along the diagonal. A 1.6 mm-diameter circle cut out of the RIS layer prevents the probe contacting from metal RIS elements. Table 1 lists the simulation antennas' parameters.

A. Single Layer Semi-Circled Linearly Polarized Antennas

The proposed antennas are designed by employing the semi-circled fractal boundary curves of different IRs, as the sides of a square patch. For linear polarization (LP) radiation of semi circled fractal boundary antennas, symmetrical fractal curves having same IR is deployed as edges of a square patch. The geometries of studied stage 1 and stage 2 antenna structures are pictured in Figures 4 and 5. The corresponding return loss characteristics of stage 1 and stage 2 of square Semi-circled fractal antennas are depicted in Figures 6 and 7.

TABLE 1
NOMINATED ANTENNAS PARAMETERS

Iteration	Geometry	Representation	Dimensions(mm) L_1=36, L_2=44, L_3=46,a_1=8, a_2=9
1	Semi-circled	IO1 Semi-circled1	h_1=0, h_2=3.2
	Semi-circled with square elements as RIS	Square RIS IO1 Semi-circled1	h_1=1.6, h_2=3.2
	Semi-circled with fractal elements as RIS	Fractal RIS IO1 Semi-circled1	h_1=1.6, h_2=3.2
2	Semi-circled	IO1 Semi-circled2	h_1=0, h_2=3.2
	Semi-circled with square elements as RIS	Square RIS IO1 Semi-circled2	h_1=1.6, h_2=3.2
	Semi-circled with fractal elements RIS	Fractal RIS IO1 Semi-circled2	h_1=1.6, h_2=3.2

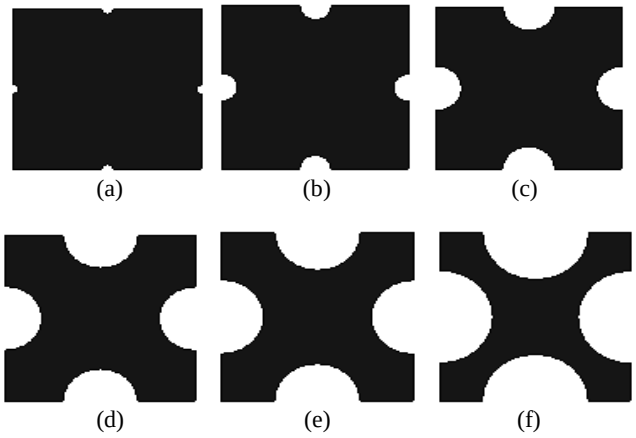

Fig. 4. Stage 1 Semi-circled LP fractal antennas with different IRs: (a) 0.055, (b) 0.16, (c) 0.27, (d) 0.38, (e) 0.44, (f) 0.55

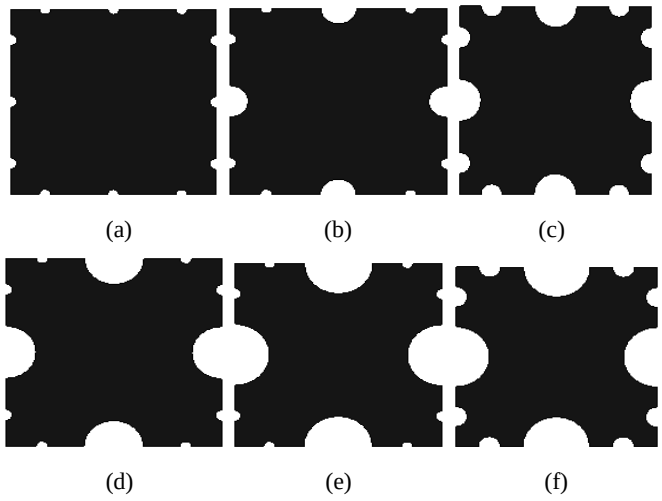

Fig. 5. Stage 2 Semi-circled LP fractal antennas with different IRs – R_1 and R_{12}: (a) 0.055 and 0.055, (b) 0.16 and 0.055, (c) 0.22 and 0.11, (d) 0.27 and 0.055, (e) 0.33 and 0.055, (f) 0.33 and 0.11

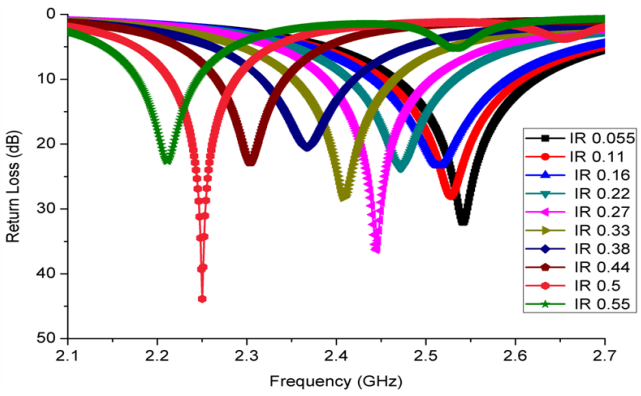

Fig. 6. Return loss characteristics of linearly polarized stage 1 Semi-circled fractal antennas with different IRs

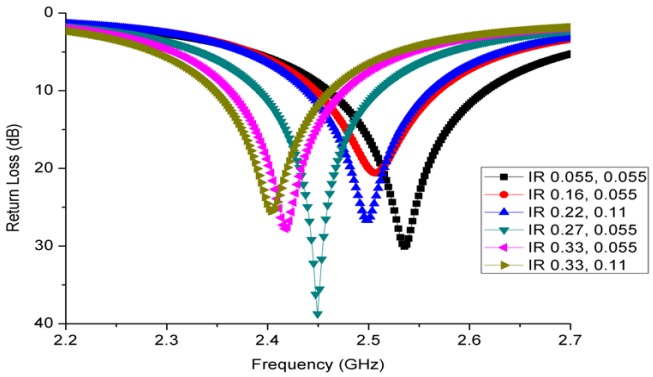

Fig. 7. Return loss characteristics of linearly polarized stage 2 Semi-circled fractal antennas with different IRs

B. Single-Layer-Semi-Circled Circularly Polarized Antennas

For circular polarization, asymmetrical semi-circled fractal curves are substituted along the square patch's edges. The geometry of the IO1 and IO2 CP antenna structures are provided in the Figures 8 and 9. The corresponding simulation findings are shown in the Figures 10 and 11. The respective axial ratio plots are depicted in Figures 12 and 13.

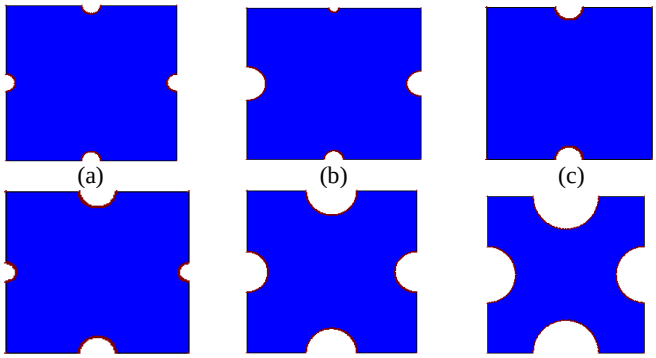

Fig. 8. The proposed antennas geometries of Semi-circled patch: (a) Semi circled linearly polarized antenna 1 : IR - R_{x1} = 0.11, (b) Semi circled CP antenna 2: IRs - R_{x1} = 0.15, R_{x2} = 0.2, R_{y1} = 0.05, R_{y2} = 0.1, (c) Semi circled CP antenna 3 : IRs - R_{x1} = 0, R_{y1} = 0.16, (d) Semi circled CP antenna 4 : IRs - R_{x1} = 0.11, R_{y1} = 0.2, (e) Semi circled CP antenna 5 : IRs - R_{x1} = 0.25, R_{y1} = 0.3, (f) Semi circled CP antenna 5 : IRs - R_{x1} = 0.33, R_{y1} = 0.44

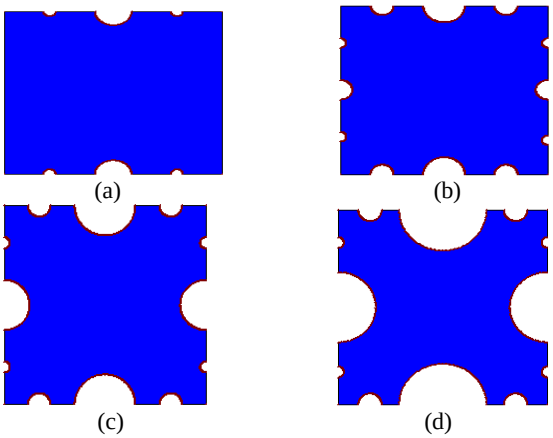

Fig. 9. The proposed antennas geometries of Semi-circled stage 2 patch: (a) Semi circled stage 2 CP antenna 1 : IRs - R_{x1} = 0, R_{y1} = 0.16 and R_{x12} = 0, R_{y12} = 0.055, (b) Semi circled stage 2 CP antenna 2 : IRs - R_{x1} = 0.11, R_{y1} = 0.2 and R_{x12} = 0.055, R_{y12} = 0.11, (c) Semi circled stage 2 CP antenna 3 : IRs - R_{x1} = 0.25, R_{y1} = 0.3 and R_{x12} = 0.055, R_{y12} = 0.11, (d) Semi circled stage 2 CP antenna 4 : IRs - R_{x1} = 0.33, R_{y1} = 0.44 and R_{x12} = 0.055, R_{y12} = 0.11

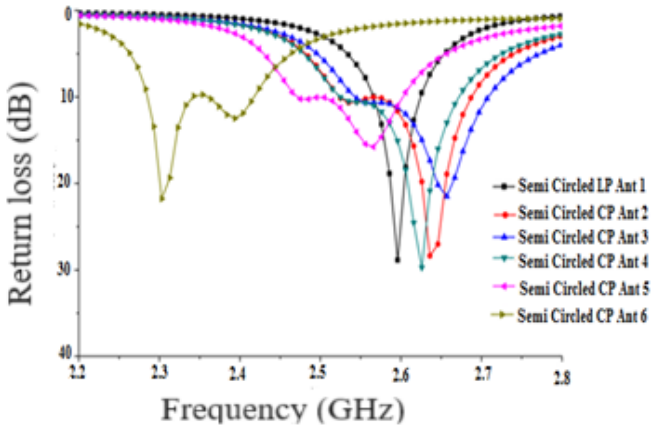

Fig. 10. Return loss characteristics of IO 1 Semi-circled CP fractal antennas with different IRs

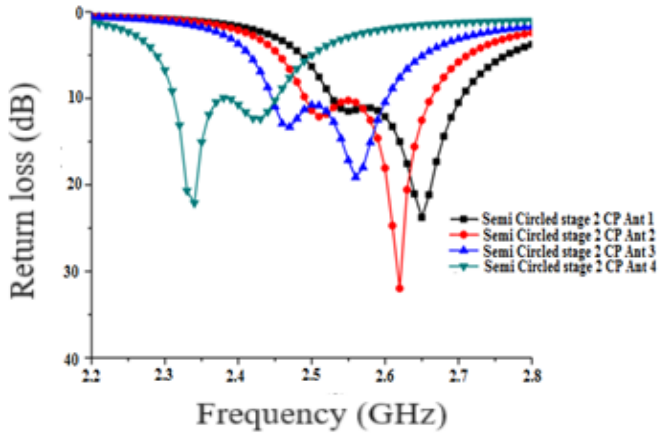

Fig. 11. Return loss characteristics of IO 2 Semi-circled CP fractal antennas with different IRs

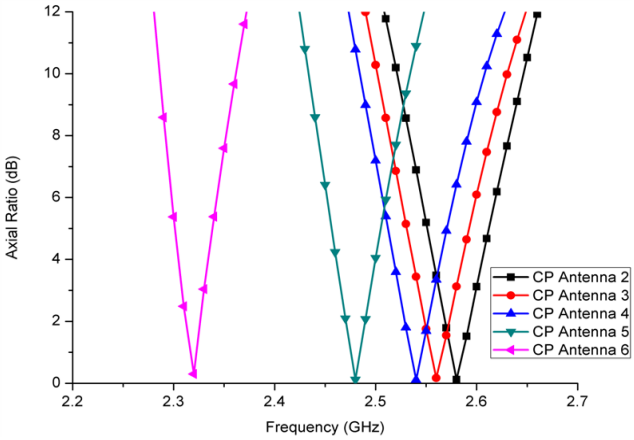

Fig. 12. Axial ratio characteristics of IO 1 Semi-circled CP fractal antennas with different IRs

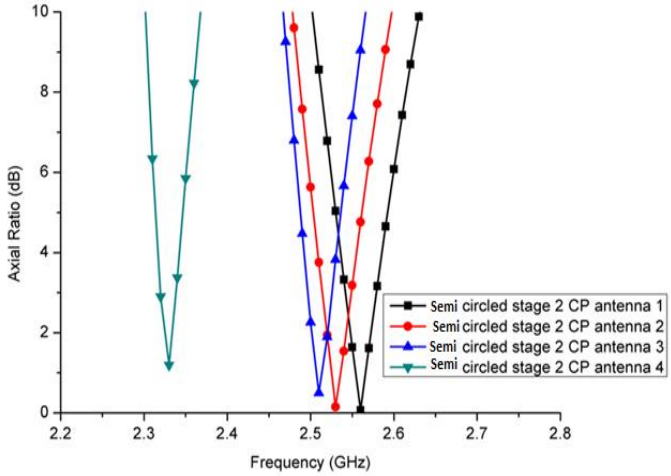

Fig. 13. Axial ratio characteristics of IO 2 Semi-circled CP fractal antennas with different IRs

C. RIS-based Semi-circled Fractal Boundary Antennas

To increase the bandwidth, semi-circled patches are placed over RIS. They are initially investigated in comparison to RIS square elements. Figure 14 shows the RIS-based semi-circled antennas that are being presented.

TABLE 2
THE PROPOSED ANTENNA PARAMETERS

Iteration	Geometry	Representation	R-along x and y axes
1	Semi-circled with square elements as RIS	Square RIS IO1 Semi-circled 1	0.2, 0.11
	Semi-circled with fractal elements as RIS	Fractal RIS IO1 Semi-circled 1	
2	Semi-circled with square elements as RIS	Square RIS IO1 Semi-circled 2	0.3, 0.25
	Semi-circled with fractal elements as RIS	Fractal RIS IO1 Semi-circled 2	

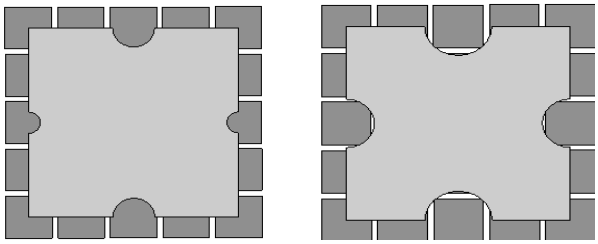

(a) (b)

Fig. 14. The proposed Semi-circled antennas over square RIS elements: (a) Square RIS Semi-circled 1, (b) Square RIS Semi-circled 2

Figures 15 and 16 shows the related return loss and axial ratio charts, respectively. Table 2 lists the proposed antenna structures. In order to further increase bandwidth, semi-circled fractal RIS elements are later used in place of square RIS elements; the corresponding structures are depicted in Fig. 17 and the relevant return loss plots are shown in Fig. 18. Fig. 19 shows the vector current distribution on the fractal RIS antenna. Table 3 provides a summary of the simulation findings for the RIS-based semi-circled antennas.

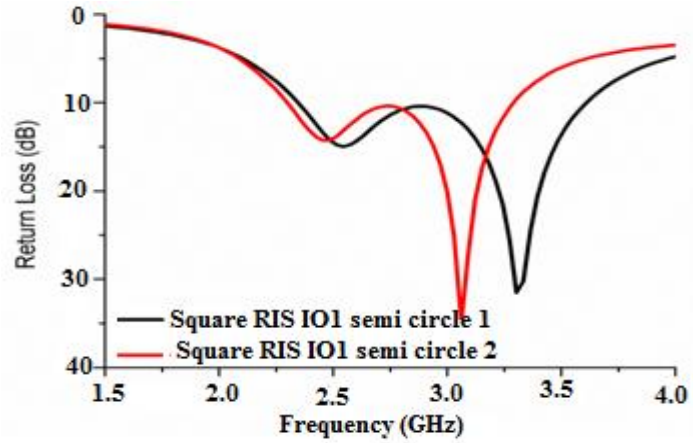

Fig. 15. The return loss characteristics of square RIS Semi-circled antennas

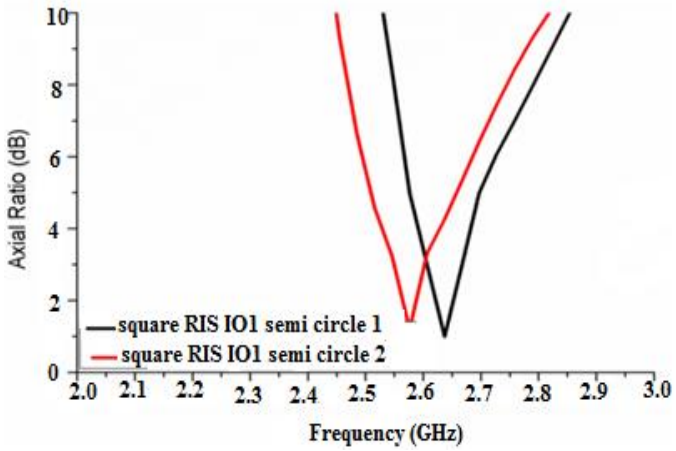

Fig. 16. The simulated axial ratio characteristics of square RIS Semi-circled antennas

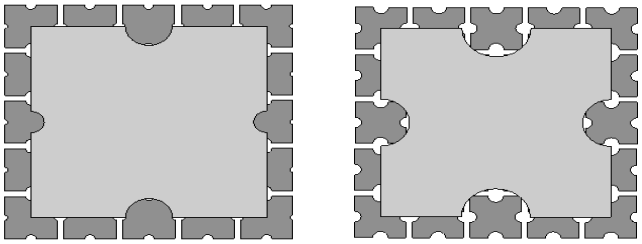

(a) (b)

Fig. 17. Semi-circled antennas over fractal RIS: (a) Fractal RIS Semi-circled 1, (b) Fractal RIS Semi-circled 2

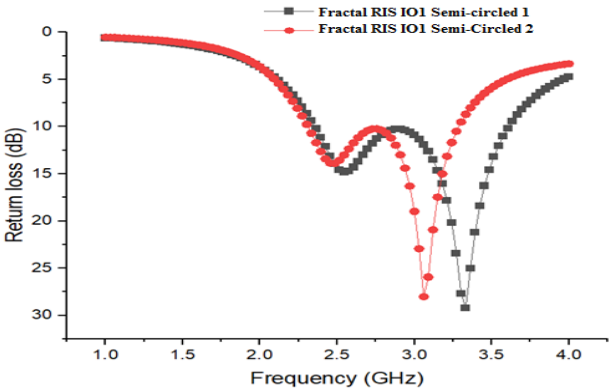

Fig. 18. The simulated return loss characteristics of fractal RIS Semi-circled antennas

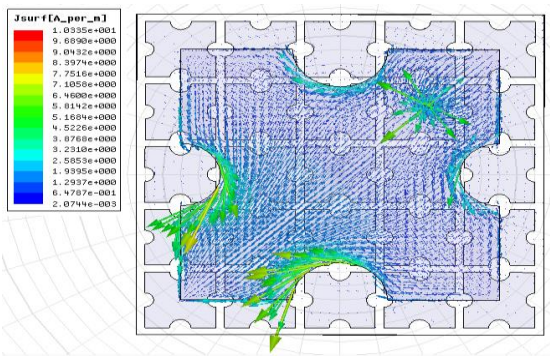

Fig. 19. The surface current distribution of fractal RIS IO1 semi circled 1

TABLE 3
THE PROPOSED RIS-BASED ANTENNA SIMULATION SUMMARY

IO	Antenna	10-dB Return loss		3-dB Axial ratio	
		Frequency range (GHz)	Band width (%)	Frequency range (GHz)	Band width (%)
1	Square RIS IO1 Semi-circled 1	2.35-3.6	42.01	2.6-2.66	2.28
	Fractal RIS IO1 Semi-circled 1	2.36-3.63	42.4	2.66-2.79	4.77
2	Square RIS IO1 Semi-circled 2	2.30 - 3.28	35.12	2.54-2.6	2.33
	Fractal RIS IO1 Semi-circled 2	2.33 - 3.27	33.57	2.53-2.61	3.11

D. Meta-Material Based Multiband Antenna

To get the multiband operation, a mush room unit cell is embedded in the semi-circled boundary patch. The mush room unit cell consists of a 45^0 rotated and scaled down patch with a via connected between the rotated patch and ground plane. In order to avoid contact with RIS elements, a circular area is etched at that location on RIS elements. The proposed antennas are displayed in Fig. 20 and the respective return loss curves are depicted in Fig. 21. The proposed multiband antenna operating at 2.4 GHz and 3.4 GHz is useful for WLAN and Wi-MAX applications correspondingly.

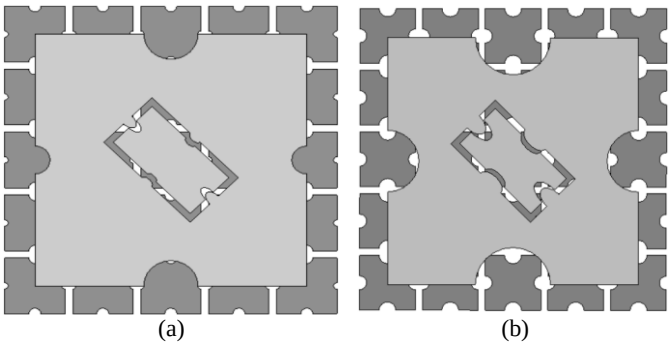

(a) (b)

Fig. 20. Metamaterial loaded multiband antennas

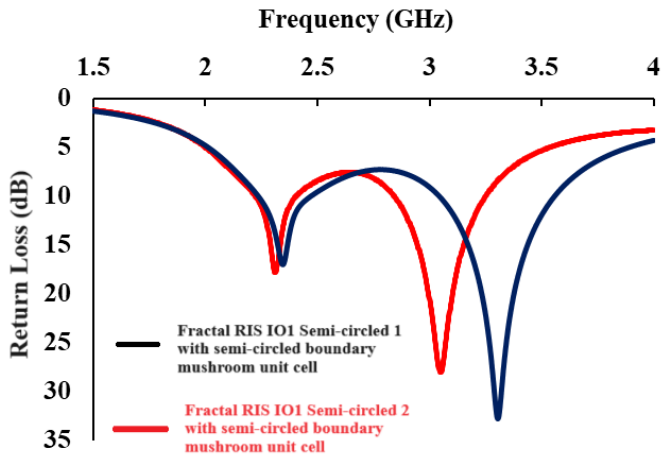

Fig. 21. Return loss characteristics of Multiband antennas

IV. MEASURED RESULTS

A fractal RIS semi-circled antenna is constructed, and tests are conducted, in order to verify the simulation's findings. Figure 22 displays the corresponding manufactured antenna. A two-layer antenna is used. RIS elements are printed on the bottom layer's 1.6 mm thickness of FR4 epoxy, which has a dielectric constant of 4.4. On 3.2 mm thick RT/ Duroid 5880 with a dielectric constant of 2.2, the top layer is printed with a semi-circled fractal. A dielectric adhesive is used to stack the two layers. Figure 23 shows the contrast between the proposed antenna's measured and simulated performance. The discrepancies between the results of simulation and experiment are caused by tolerance levels used in the antenna's manufacturing. Table 4 provides the comparison of proposed antenna with the existing literature.

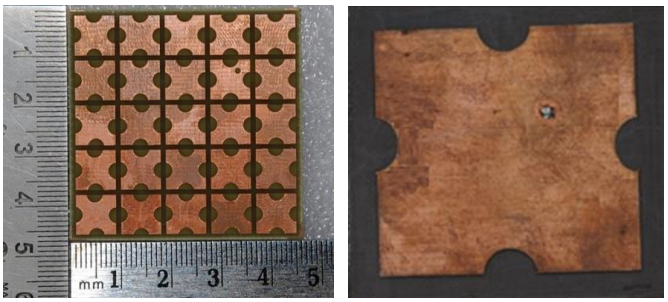

(a) (b)

Fig. 22. Fabricated antenna: (a) Semi-circled RIS, (b) semi-circled fractal antenna

TABLE 4
THE COMPARISON OF PROPOSED MULTI BAND ANTENNA WITH EXISTING LITERATURE

S.No.	Ref.	Operating bands (GHz)	10-dB return loss Bandwidth (%)
1.	[3]	Lower band: 2.32 - 2.42	4.2
		Upper band: 2.7 - 2.75	2
2.	[15]	Lower band: 2.24-2.38	6.06
		Upper band: 2.54-2.58	1.56
3.	[16]	Lower band: 2.4	<1
		Upper band: 3.01-3.27	8.22
4.	[17]	Lower band: 2.30-2.36	2.59
		Upper band: 3.21-3.49	8.48
5.	Proposed	Lower band: 2.2-2.7	20.4
		Upper band: 3.0-3.6	18.18

As per the comparison table, it is observed that the proposed antenna exhibits multiband operation at WLAN and Wi-MAX applications. The antenna is carefully designed in such a way that to operate at WLAN and Wi-MAX bands. Impedance bandwidth improved at both the bands significantly, it is due to the insertion of 45^0 rotated fractal mushroom unit cell at the centre of the RIS based fractal patch. As it is generating high bandwidth at the both the bands, the proposed antenna very much suitable for the WLAN and Wi-MAX applications.

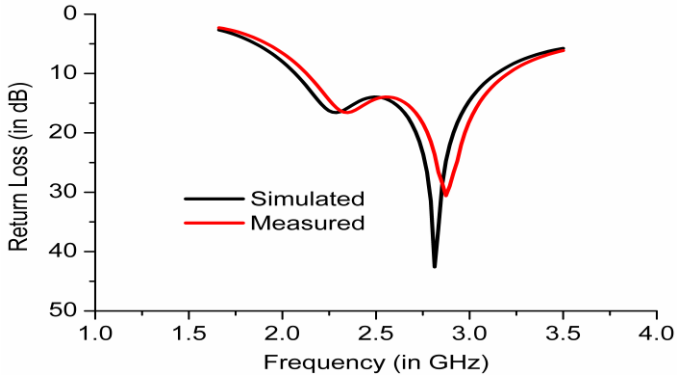

(a)

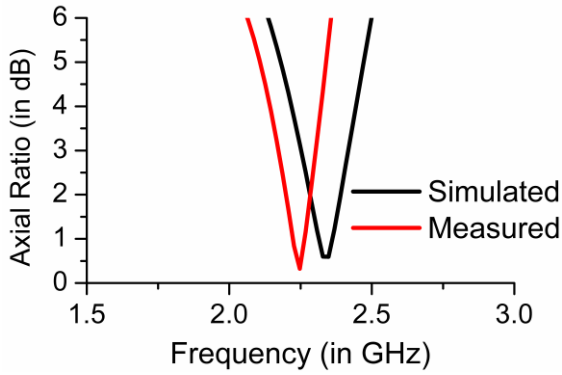

(b)

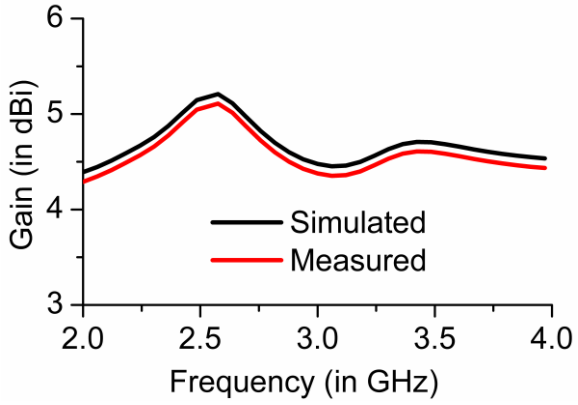

(c)

Fig. 23. Simulated and measured results comparison: (a) Return loss characteristics, (b) Axial ratio, and (c) Gain

V. Conclusion

Through simulations and experimentation, a broadband semi-circled antenna is thoroughly examined. For the best generation of bandwidth, the RIS elements are optimised to a 5×5 configuration. The effects of CP radiation are investigated for a semi-circled fractal with square elements RIS, and fractal elements RIS. Impedance matching has been observed to be achieved over a wider bandwidth with the usage of optimised fractal RIS elements. For multiband operation RIS with mush room cell is implemented. The proposed multiband antenna operates at WLAN and Wi-MAX frequency bands and exhibits broad impedance bandwidth at both the bands. The nominated structure is beneficial for wireless ISM band application. The proposed RIS antenna exhibits high CP bandwidth. The presented multiband antenna generates wide impedance bandwidth at both the operating bands as compared to the existing designs found in the literature.

References

[1] C. Milias, R. B. Andersen, P. I. Lazaridis, Z. D. Zaharis, B. Muhammad, J. T. B. Kristensen, A. Mihovska and D.S. Hermansen, **"**Metamaterial-Inspired Antennas: A Review of the State of the Art and Future Design Challenges**"**, in *IEEE Access*, vol. 9, pp. 89846-89865, June 2021, DOI: 10.1109/ACCESS.2021.3091479

[2] S. Abdullah, G. Xiao and R. E. Amaya, **"**A Review on the History and Current Literature of Metamaterials and its Applications to Antennas & Radio Frequency Identification (RFID) Devices**"**, in *IEEE Journal of Radio Frequency Identification.*, vol. 5, no. 4, pp. 427-445, Dec. 2021, DOI: 10.1109/JRFID.2021.3091962

[3] C. G. M. Ryan and G. V. Eleftheriades, **"**Single- and Dual-Band Transparent Circularly Polarized Patch Antennas With Metamaterial Loading**"**, in *IEEE Antennas Wireless Propagation Letters*, vol. 14, pp. 470-473, Nov. 2014, DOI: 10.1109/LAWP.2014.2368115

[4] W. E. I. Liu, Z. N. Chen, X. Qing, J. Shi and F. H. Lin, **"**Miniaturized Wideband Metasurface Antennas**"**, in *IEEE Transactions on Antennas and Propagation*, vol. 65, no. 12, pp. 7345-7349, October 2017, DOI: 10.1109/TAP.2017.2761550

[5] W. Cao, B. Zhang, J. Jin, W. Zhong and W. Hong, **"**Microstrip Antenna With Electrically Large Property Based on Metamaterial Inclusions**"**, in *IEEE Transactions on Antennas and Propagation*, vol. 65, no. 6, pp. 2899-2905, April 2017, DOI: 10.1109/TAP.2017.2694466

[6] J. Chatterjee, A. Mohan and V. Dixit, **"**Broadband Circularly Polarized H-Shaped Patch Antenna Using Reactive Impedance Surface**"**, in *IEEE Antennas and Wireless Propagation Letters*, vol. 17, no. 4, pp. 625-628, April 2018, DOI: 10.1109/LAWP.2018.2806993

[7] M. Li, Y. Zhang and M.-C. Tang, **"**Design of a Compact Wideband Bidirectional Antenna Using Index-Gradient Patches**"**, in *IEEE Antennas and Wireless Propagation Letters*, vol. 17, no. 7, pp. 1218-1222, July 2018, DOI: 10.1109/LAWP.2018.2839900

[8] Q. Chen, H. Zhang, Y.-J. Shao and T. Zhong, **"**Bandwidth and Gain Improvement of an L-Shaped Slot Antenna With Metamaterial Loading**"**, in *IEEE Antennas and Wireless Propagation Letters*, vol. 17, no. 8, pp. 1411-1415, August 2018, DOI: 10.1109/LAWP.2018.2848639

[9] Y. Pan and Y. Dong, **"**Low-Profile Low-Cost Ultrawideband Circularly Polarized Slot Antennas**"**, in *IEEE Access*, vol. 7, pp. 160696-160704, October 2019, DOI: 10.1109/ACCESS.2019.2950521

[10] W. Cao, W. Ma, W. Peng and Z. Chen, **"**Bandwidth-Enhanced Electrically Large Microstrip Antenna Loaded With SRR Structures**"**, in *IEEE Antennas and Wireless Propagation Letters*, vol. 18, no. 4, pp. 576-580, April 2019, DOI: 10.1109/LAWP.2019.2896384

[11] K. Zhang, G. A. E. Vandenbosch and S. Yan, **"**A Novel Design Approach for Compact Wearable Antennas Based on Metasurfaces**"**, in *IEEE Transactions on Biomedical Circuits Systems.*, vol. 14, no. 4, pp. 918-927, Aug. 2020, DOI: 10.1109/TBCAS.2020.3010259

[12] W. Wan, M. Xue, L. Cao, T. Ye and Q. Wang, **"**Low-Profile Broadband Patch-Driven Metasurface Antenna**"**, in *IEEE*

Antennas and Wireless Propagation Letters, vol. 19, no. 7, pp. 1251-1255, July 2020, DOI: 10.1109/LAWP.2020.2997346

[13] Z. Wang, Y. Dong, Y. Ning and T. Itoh, **"**Miniaturized Circularly Polarized Periodically Structured Surface Antenna for RFID Application Inspired by SRR**"**, in *IEEE Transactions on Antennas and Propagation*, vol. 69, no. 11, pp. 7269-7277, November 2021, DOI: 10.1109/TAP.2021.3075720

[14] X. Wu, X. Wen, J. Yang, S. Yang and J. Xu, **"**Metamaterial Structure Based Dual-Band Antenna for WLAN**"**, in *IEEE Photonics Journal*, vol. 14, no. 2, pp. 1-5, April 2022, DOI: 10.1109/JPHOT.2022.3163170

[15] N. Suman and N. V. S. N. Sarma, "Dual Band Circular Patch Based on Metamaterials", in *International Journal of Advances in Microwave Technology* (*IJAMT*), vol. 3, no. 2, pp. 152-155, May 2018.

[16] N. Suman and N. V. S. N. Sarma, "CSRR Based Patch Antenna for Wi-Fi and Wi-MAX Applications", in *Advanced Electromagnetics*, vol. 7, no. 3, pp. 40-45, Aug. 2018, DOI: https://doi.org/10.7716/aem.v7i3.700

[17] N. Suman and N. V. S. N. Sarma, "A Compact Microstrip Patch Antenna Based on Metamaterials for Wi-Fi and WiMAX Applications", in *Journal of Electromagnetic Engineering and Science*, vol. 18, no. 3, pp. 182-187, June 2018, DOI:10.26866/jees.2018.18.3.182